Environmental Science and Ecotechnology 9 (2022) 100143

Contents lists available at ScienceDirect

Environmental Science and Ecotechnology

journal homepage: www.journals.elsevier.com/environmental-science-and-ecotechnology/

Original Research

Carbamazepine degradation by visible-light-driven photocatalyst Ag_3PO_4/GO: Mechanism and pathway

Guanhan Chen [a], Wenyi Dong [a, b, c], Hongjie Wang [a, b, c], Zilong Zhao [a, b, *], Feng Wang [a], Feifei Wang [a], Cesar Nieto-Delgado [d, **]

[a] School of Civil and Environmental Engineering, Harbin Institute of Technology Shenzhen, Shenzhen, 518055, PR China
[b] Shenzhen Key Laboratory of Water Resource Utilization and Environmental Pollution Control, Shenzhen, 518055, PR China
[c] State Key Laboratory of Urban Water Resource and Environment, School of Environment, Harbin Institute of Technology, Harbin, 150090, PR China
[d] División de Ciencias Ambientales, Instituto Potosino de Investigación Científica y Tecnológica, IPICyT. Camino a la Presa San Jose 2055. San Luis Potosí, SLP 78216, Mexico

ARTICLE INFO

Article history:
Received 29 September 2021
Received in revised form
13 December 2021
Accepted 14 December 2021

Keywords:
Carbamazepine
Ag_3PO_4/GO
Visible light
Photocatalysis

ABSTRACT

Carbamazepine (CBZ), as one of the most frequently detected pharmaceuticals, is of great concern due to its potential impact on the ecosystem and human health. This study provides an effective approach to remove CBZ by using photocatalyst silver phosphate combined with graphene oxide (Ag_3PO_4/GO) under visible irradiation. The morphology, composition, and optical properties of Ag_3PO_4/GO were characterized employing SEM, XRD, and DRS. Graphene oxide could improve the visible-light utilization and promote electron's charge to enhance the photocatalytic performance of Ag_3PO_4/GO. With the optimal reaction condition of 5.86 mW/cm^2 light intensity, 15–25 °C temperature, 5–7 pH, and 0.5 mg/L catalytic dosages, 5 mg/L CBZ could be completely degraded in 30 min, and the apparent rate constant could reach 0.12 min^{-1}. Additionally, the radical trapping experiments indicated •OH and O_2^-• were the main reactive oxygen species employed to eliminate CBZ. The decay pathways of CBZ had been proposed accordingly, and the main product was the low-molecular products.

1. Introduction

Micropollutants such as pharmaceuticals are of great concern because of their potential impact on aquatic environments [1]. Carbamazepine (CBZ), a common psychiatric drug, was consumed more than 1000 tons per year [2]. Since CBZ is a nitrogen-containing aromatic heterocyclic compound with an asymmetrical structure [3], CBZ, as a non-biodegradative material, becomes one of the most frequently detected pharmaceuticals, which has been observed in surface water [4], wastewater [5], and drinking water [6]. The concentration of CBZ in seawater could be up to a few ug/L, while up to a few ng/g dry weight in bivalves' tissues [7]. Besides, CBZ and its derivates were toxic to aquatic life, including algae [8], daphnia magna [9], and fish embryos [10], etc. CBZ has a potential chronic effect on the algal cell disturbing specific proteins to damage membrane function [8]. Thus, it is urgent to remove CBZ in an aqueous environment.

Advanced oxidation process (AOPs) is proved to be an effective way to deal with the refractory organic pollutants as well as CBZ, rather than membrane filter, adsorption, biochemical, etc [11–13]. However, membrane fouling, high-cost regeneration, long-period operation, and low removal rate hinder the practical application. For instance, CBZ could not be removed effectively or even accumulated after the sewage treatment plant contained primary clarifier, activated sludge process, and final clarifier [14]. Photocatalysis, one of the widely studied AOPs, has been considered a promising technology to treat non-biodegradable and toxic pollutants in water and wastewater due to energy conservation and simple operation. However, the low photocatalytic rate and limited light utilization of many photocatalysts hindered the widely-used application of wastewater treatment. For instance, the pseudo-first-order rate constant (0.0237 min^{-1}) shown by BiOCl

* Corresponding author. School of Civil and Environmental Engineering, Harbin Institute of Technology Shenzhen, Shenzhen, 518055, PR China.
** Corresponding author.
E-mail addresses: berthillon@hotmail.com (Z. Zhao), cesar.nieto@ipicyt.edu.mx (C. Nieto-Delgado).

https://doi.org/10.1016/j.ese.2021.100143

suggested that it needed more than 150 min to remove CBZ completely [15]. Besides, some photocatalysts lacked visible-light utilization, which hindered their practical application. For example, Nd-doped Sb_2O_3/TiO_2 degraded CBZ under UVC light [16], while UV accounts for a small fraction of the total solar energy [17]. Thus, it is crucial to develop a visible photocatalyst for CBZ degradation with a high degradation rate.

In particular, silver phosphate (Ag_3PO_4) has been attached much attention due to its high photocatalytic performance and visible light utilization. Ag_3PO_4 has a remarkable quantum efficiency of up to 90% during the photodecomposition of organic dye under visible light. Moreover, Ag_3PO_4 has a bandgap of 2.43 eV, which makes it potential for using as a visible-light-driven photocatalyst [18,19]. However, the photo-corrosion of Ag_3PO_4 hinders the application of wastewater treatment [20]. Thus, Ag_3PO_4 was combined with semiconductors, heteroatoms, carbonaceous material, etc. Graphene oxide (GO), a wonder material, in particular, has emerged as compelling semiconductor support because of its superlative properties, such as large specific area and excellent electronic conductivity [21]. Combined with graphene oxide, the charge recombination of Ag_3PO_4 is expected to be suppressed, and the catalytic performance further improved, which has been reported previously [22]. Moreover, cyclic aromatic hydrocarbons (e.g., naphthalene, phenanthrene, and pyrene) could be removed effectively by photocatalyst Ag_3PO_4/GO [23], while CBZ, as a fused heterocycle compound, has a similar aromatic structure. However, the performance and mechanism of CBZ degradation by using Ag_3PO_4/GO was seldomly reported. Thus, it is crucial to evaluate the performance and propose the mechanism of CBZ degradation by using photocatalyst Ag_3PO_4/GO.

Herein, a high-rate method for CBZ degradation by using visible photocatalyst Ag_3PO_4/GO was developed. CBZ could be effectively removed, while GO could enhance photocatalytic performance. In this study, we characterized the morphology, composition and optical property of Ag_3PO_4/GO, and optimized the experiment conditions (light intensity, reaction temperature, initial pH, and catalytic dosage). Moreover, the catalytic mechanism of CBZ degradation by Ag_3PO_4/GO was comprehensively studied and proposed. We have provided a facile, efficient, and sustainable approach for the remediation of CBZ and shed light on the remediation of refractory organic pollutants.

2. Experimental sections

2.1. Materials and chemicals

Graphene oxide was purchased from Ashine Advanced Carbon Materials (Changzhou) Co., Ltd. Silver nitrate ($AgNO_3$) was obtained from Sinopharm Chemical Reagent Co., Ltd (Shanghai, China). Carbamazepine ($C_{15}H_{12}N_2O$) isopropanol (IPA), benzoquinone (BQ), potassium iodide (KI), and sodium phosphate dibasic dodecahydrate ($Na_2HPO_4{\cdot}12H_2O$) were provided by Aladdin Chemistry Co. Ltd (Shanghai, China). All chemicals were of analytical grade, and deionized water was used in all the experiments unless specified. In addition, the morphology and composition of GO, such as the spectra of the scanning electron microscope (SEM), atomic force microscopic (AFM), Fourier transform infrared reflection (FTIR), and Raman, were shown in Fig. S1.

2.2. Preparation of Ag_3PO_4/GO

Typically, silver phosphate was prepared by the precipitation method. A certain amount of silver nitrate ($AgNO_3$) solution dropped slowly into 10 mL graphene oxide (GO) dispersion (1 mg/mL), followed by 30 min sonication. Then, a certain amount of Na_2HPO_4 solution was dropped into the above solution and stirred for 4 h. AGO-1.0 was obtained after removing the supernatant and 60° oven-dried. According to the content of GO (0.5, 2.0, 4.0 mg/mL), the obtained catalysts were named AGO-0.5, AGO-2.0, AGO-4.0. The pristine silver phosphate (Ag_3PO_4) was synthesized by the same process without adding GO.

2.3. Degradation experiments of CBZ by Ag_3PO_4/GO

The photocatalytic activity of the sample was appraised by CBZ degradation under visible light irradiation. PCX50C Discover multichannel photocatalytic reaction system (Beijing Perfectlight Technology Co., China) was employed as a visible light source with a wavelength longer than 420 nm. Typically, a certain amount of photocatalyst and 50 mL CBZ solution (5 mg/L) were mixed in a jacketed beaker, and after 5 min sonication, the suspension was stirred for 30 min in the dark to establish an adsorption-desorption equilibrium. The beaker was enclosed by a water circulation system to maintain the temperature during light illumination. At the given time intervals, 1 mL of the suspension was collected and centrifuged to remove the photocatalyst in the dark.

2.4. Analysis and characterizations

Ultra-high-performance liquid chromatography (Waters, USA) equipped with a Symmetry C18 column (100 mm × 2.1 mm × 1.7 μm, Waters, USA) and a Photodiode Array (PDA) detector (Waters, USA) was adopted to determine the CBZ concentration in the collected solution. The measurement was performed at a flow rate of 0.25 mL/min with the mobile phase (methanol: 0.1 %formic acid = 6:4, v/v), and CBZ was detected at $\lambda = 285$ nm. The transformation products (TPs) of CBZ were identified by UPLC/Triple Quad mass spectrometry (Water H-Class & XEVO, USA) in the positive ESI mode. Solvent A (ultrapure water) and B (acetonitrile) were used as the mobile phase, and the flow was 0.5 mL/min. The gradient elution was operated as follows: 0−1 min, 5−20% A; 1−8 min, 20−95% A; 8−9min, 95-5% A; 9−10 min, 5% A.

The X-ray diffraction (XRD) patterns of the obtained samples were tested on a diffractometer (Rigaku Smartlab, Japan) with Cu Kα source, in the 2θ range of 10−80°. The morphology of the products was measured by SEM (Hitachi SU8010) and AFM (Bruker Dimension Icon). A diffusive reflective UV−vis spectrophotometer (DRS, Shimadzu, UV3600 plus) was employed to measure the UV−vis absorption and estimate the bandgap of the catalysts. The photoluminescence (PL) spectra of samples were tested by Hitachi F-7100 spectrofluorometer. The Raman spectra were measured by a spectrometer (Horiba Scientific LabRAM HR Evolution). The electron spin resonance (ESR) spectra were recorded on a Bruker A300 electron paramagnetic resonance spectrometer. BET surface area was measured by nitrogen adsorption-desorption curve using Micromeritics ASAP 2020 system. The FTIR was carried on a spectrometer (Shimadzu IRAffinity-1, Japan). Raman spectra were obtained using a LabRAM HR Evolution (Horiba Scientific LabRAM HR Evolution, France) with laser excitation at 514 nm.

3. Results and discussions

3.1. Characterization of Ag_3PO_4/GO

The morphology and size of catalyst pristine Ag_3PO_4 and AGO-1.0 are shown in Fig. 1. Pristine Ag_3PO_4 exhibited irregular spherical morphology and non-uniform diameters, and the particle size mainly lay in the range of 1.2−2.4 μm. Also, some aggregation phenomena could be observed (Fig. 1a and c). Mixed with graphene

oxide, AGO-1.0 showed uniform particles, and the size was decreased to 200 nm–600 nm (Fig. 1b and d). GO could control the growth of Ag_3PO_4 due to the electrostatic interaction between Ag^+ and GO sheets [24]. In addition, GO could enhance the reaction sites for catalysts due to its high surface area. Combined with GO (6.61 m^2/g), AGO-1.0 (2.97 m^2/g) showed a larger specific surface area than that of Ag_3PO_4 (2.22 m^2/g). Besides, Fig. S2 shows that Ag, P, and O elements of AGO-1.0 are uniformly distributed in the selected area, indicating that GO mixed well with Ag_3PO_4. Thus, adding GO would be beneficial to design the photocatalyst.

The XRD spectra were recorded to study the phase composition of Ag_3PO_4, AGO-1.0, and GO. As shown in Fig. 2a, the diffraction peaks of Ag_3PO_4 and AGO-1.0 were well indexed to the body-centered cubic structure of Ag_3PO_4 with high crystallinity (JCPDS No.06-0505). And the XRD pattern of GO displayed a dominated diffraction peak at around $2\theta = 9.32^\circ$, which corresponds to a d-spacing of 0.83 nm in the lamellar structure of GO, illustrating that pristine graphite was fully oxide into GO sheets. In addition, the apparent diffraction peak at around $2\theta = 9.32^\circ$ of GO sheets was not disclosed in the pattern of AGO-1.0, demonstrating that the addition of GO sheets does not influence the phase and crystal structure of Ag_3PO_4. The Raman spectra of catalyst Ag_3PO_4 and AGO-1.0 were performed, as shown in Fig. 2b. For Ag_3PO_4, the peaks at 905 and 999 cm^{-1} were observed, which was consistent with the previous reports [25]. While for AGO-1.0, the peaks of graphene oxide at 1357 and 1605 cm^{-1} were observed [26], which further confirms the generation of AGO-1.0 composites.

To evaluate the optical properties of AGO-1.0, UV–vis spectra were performed, and the results are shown in Fig. 3a. The light absorption edge of pure Ag_3PO_4 is about 525 nm, which agrees with the previous reports [27]. The coupling GO with Ag_3PO_4 induced a red shit of band edge, while the visible light absorption of AGO-1.0 enhanced significantly. According to the Kubelka-Munk method, the bandgap energy (Eg) for Ag_3PO_4 and AGO-1.0 was estimated to be 2.4 and 2.3 eV, respectively, while Ag_3PO_4 is an indirect semiconductor [19]. The presence of GO would promote the visible light absorption of AGO-1.0 and boost the utilization efficiency of visible light.

To examine the recombination rate of photogenerated carriers of the as-prepared samples, the PL analysis was conducted, as shown in Fig. 3b. The PL intensity was determined by giving an excitation wavelength of 325 nm. A stronger PL emission peak presented the rapid recombination of electron-hole pairs and the poorest photocatalytic efficiency [28]. AGO-1.0 exhibited a lower intensity than Ag_3PO_4, indicating the higher separation efficiency of electron-hole pairs in AGO-1.0. Therefore, GO could effectively suppress the recombination of photogenerated electrons and holes of AGO-1.0.

3.2. CBZ degradation by photocatalyst Ag_3PO_4/GO

3.2.1. Photocatalytic performance contrast of Ag_3PO_4 with and without GO

Fig. 4 and Fig. S3 show the photocatalytic performance of the as-prepared catalysts by monitoring the degradation of CBZ under visible light irradiation. As shown in Fig. 4a, in comparison with pristine Ag_3PO_4, AGO-1.0 composites showed superior photocatalytic activity for CBZ degradation. As for GO, the removal of CBZ mainly relied on absorption rather than degradation due to hydrophobic effects, electrostatic interactions, and π–π EDA interactions [29]. Fig. 4b shows that the photocatalytic reaction rate can be well-described by pseudo-first-order kinetics. The apparent reaction rate constant was 0.025 min^{-1} and 0.039 min^{-1} for Ag_3PO_4 and AGO-1.0, respectively. The degradation of CAZ by AGO-0.5, AGO-2.0, and AGO-4.0 was also evaluated (Fig. S3), and their k_{app} were 0.023, 0.039, and 0.040 min^{-1}, respectively. Compared to AGO-1.0, the slightly improved performance of AGO-2.0 and AGO-4.0 was due to the saturation state of Ag_3PO_4 combined with GO [30]. Thereby, the results demonstrate that the engagement of GO on the surface of Ag_3PO_4 has been proved to be an available and

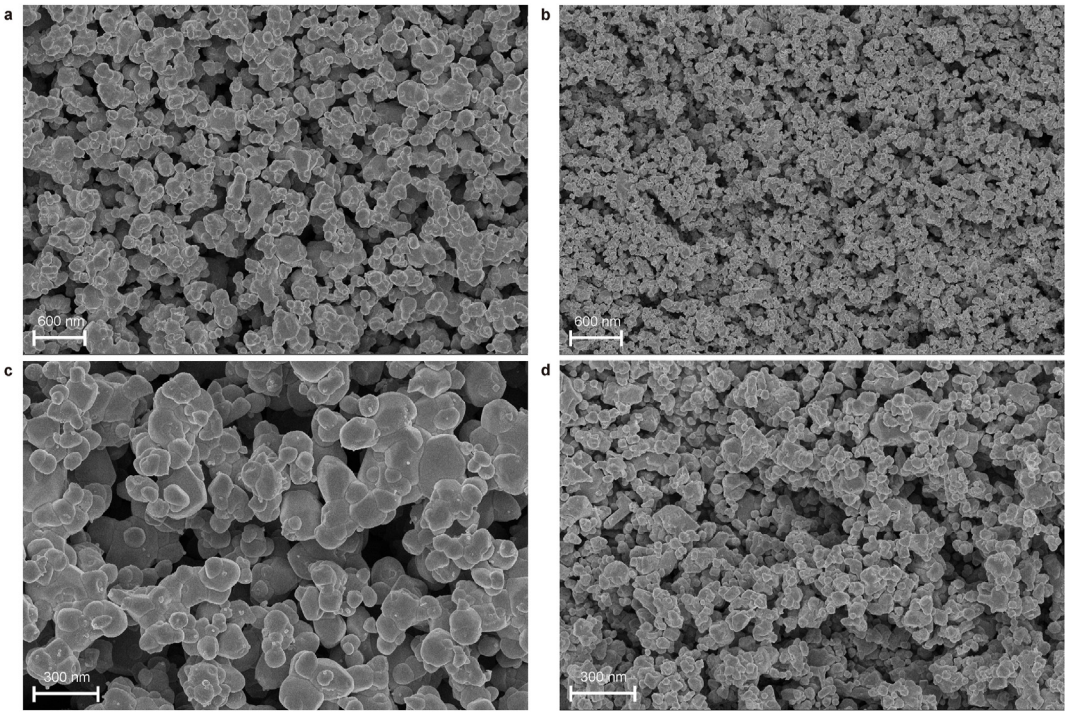

Fig. 1. SEM images of (a) Ag_3PO_4, (b) AGO-1.0, and the enlarged SEM images of (c) Ag_3PO_4 and (d) AGO-1.0.

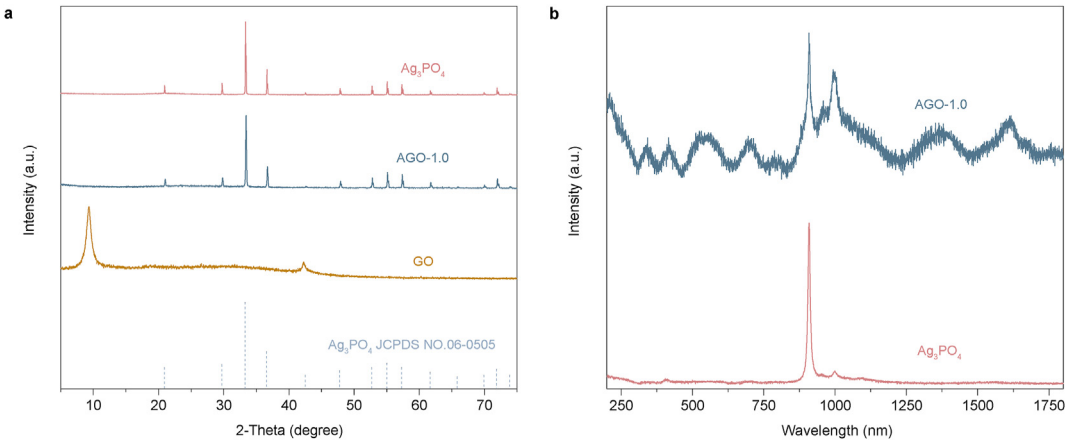

Fig. 2. (a) XRD spectra of catalyst Ag_3PO_4, AGO-1.0, and GO; (b) Raman spectra of catalyst Ag_3PO_4, and AGO-1.0.

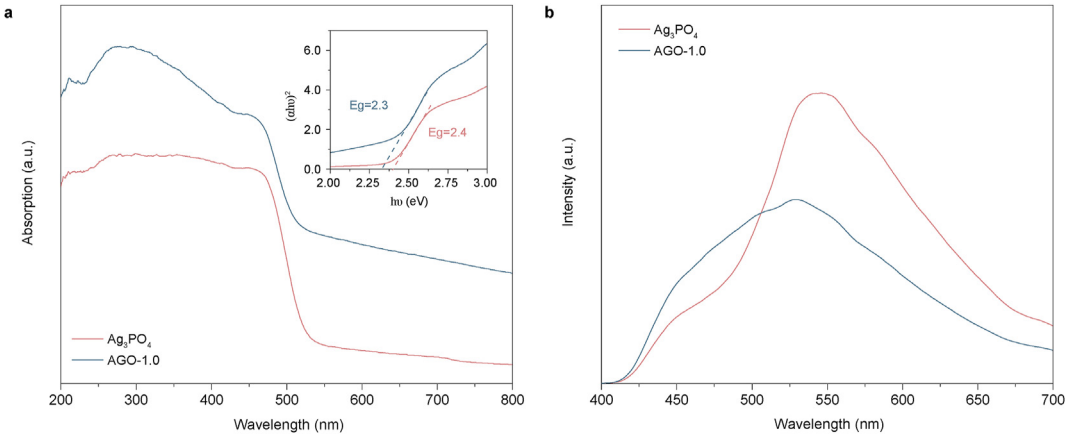

Fig. 3. The UV–vis DRS spectra (a) and PL spectra (b) of Ag_3PO_4 and AGO-1.0.

effective route for enhancing the photocatalytic performance of Ag_3PO_4. GO could promote visible-light utilization, the separation of electron-hole, and charge transfer of Ag_3PO_4.

3.2.2. Optimization of reaction condition parameters over Ag_3PO_4/GO

The effect of light intensity (1.10, 3.65, 5.86, and 7.67 mW/cm^2) on CBZ degradation efficiency and the corresponding rate constant was tested (Fig. 5a and b). As the light intensity increased from 1.10 mW/cm^2 to 5.86 mW/cm^2, the CBZ removal efficiency was

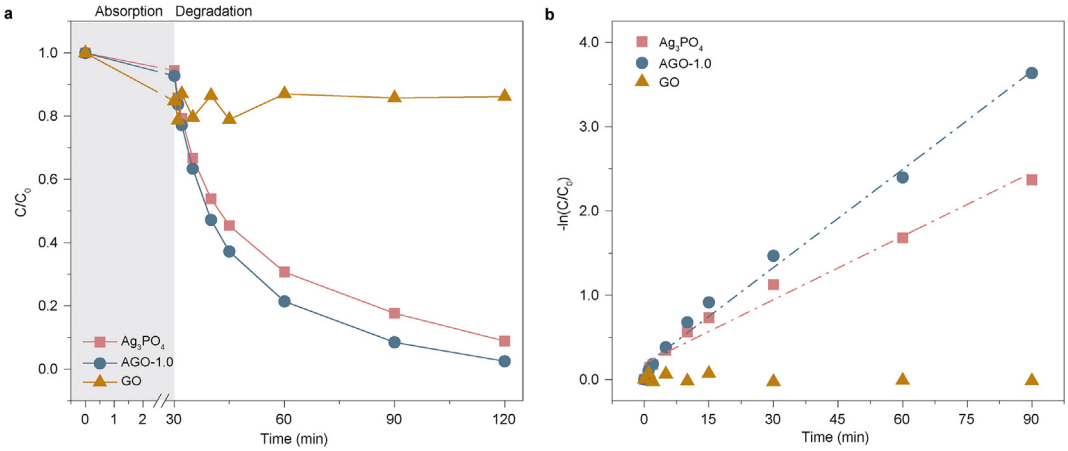

Fig. 4. (a) CBZ degradation and (b) pseudo first-order constant rate over GO, Ag_3PO_4, and AGO-1.0. (Experimental conditions: Light Intensity = 3.65 mW/cm^2, Catalytic dosage = 0.2 g/L, Reaction temperature = 25 °C, Initial pH = 6.8).

improved, while the rate constant also increased from 0.018 min^{-1} to 0.051 min^{-1}. It was because more photo-induced holes-electrons are generated as the light intensity becomes stronger. A high photon flow rate is available to attack CBZ directly and to induce oxidative species on the photocatalyst surface, thereby increasing the degradation rate [31]. However, the removal rate increased slightly as the light intensity increased to 7.67 mW/cm^2. A possible explanation may be the consumption of charge carriers by recombination, while the thermodynamically caused by high intensity favored charge carrier recombination [32,33]. Thus, considering energy conservation, 5.86 mW/cm^2 was used as the optimal light intensity for studying the effect of reaction temperature, initial pH, and catalyst dosage on CBZ degradation.

The impact of reaction temperature (15 °C, 25 °C, 35 °C, 45 °C) on the photocatalytic remediation rate under visible-irradiation was also investigated, under a photocatalyst dose of 0.2 g/L, and light intensity of 5.86 mW/cm^2. As shown in Fig. 5c&d, the CBZ removal and the rate constant declined as the temperature increased from 15 °C to 45 °C. The nature of photocatalyst and adsorption process between photocatalyst and CBZ may affect the rate of reaction, which occurs in the high temperature. On the one hand, the elevated temperature would accelerate the charge recombination [19] and reduce the stability of Ag_3PO_4 [34], which would deteriorate the catalytic activity. On the other hand, increasing temperature resulted in the serious desorption of pollutants from the catalyst surface, which was unfavorable for the photocatalytic reaction [35].

The thermodynamic parameters (standard enthalpy ($\Delta_+^+H^0$), and standard Gibbs free energy of activation ($\Delta_+^+G^0$)) were calculated as shown in Fig. S4 and Table S1, according to the transition state theory (Eqs. S1 & S2) [36]. The negative value of $\Delta_+^+H^0$ ensures the exothermic nature of the adsorption process, while the positive value of $\Delta_+^+G^0$ signified the requirement of light energy as the process is not spontaneous. Therefore, the temperature in the range of 15–25 °C is the optimal parameter for CBZ degradation.

The effect of initial pH values (3, 5, 7, 9) on photocatalytic degradation under visible irradiation was studied (Fig. 5e&f). When the pH was within the range of 5–7, a high degradation rate of CBZ was obtained, which indicated that the AGO-1.0 composite could be applied to a relatively wide range of pH. And the photocatalytic activity of AGO-1.0 was weakened sharply in the presence of excess H^+ (pH = 3) and OH^- (pH = 9). It was mainly due to the instability of Ag_3PO_4 itself, which could be dissolved or reacted in over-acid or over alkaline conditions [37]. Moreover, the initial pH of the aqueous solution might greatly affect the adsorption behavior of pollutants and the generation of ROSs during the process of photocatalytic reaction [38]. To confirm the role of initial pH on adsorption, the zeta potential of AGO-1.0 in different pH (4, 7, 10) was measured (Fig. S5). It observed that the negative value of zeta potential indicated the zero-point charge was below pH 4, and the initial pH did not influence the adsorption behavior. Hence, the pH within the range of 5–7 was the optimal initial pH for CBZ degradation.

The effect of photocatalyst dosage on the photocatalytic degradation of CBZ (5 mg/L) under visible-irradiation (3.65 mW/cm^2) was investigated (Fig. 5g and h). The photocatalytic degradation rate of CBZ increased as the photocatalytic dosage was increased from 0.2 g/L to 1.0 g/L. The degradation rate enhanced by the photocatalyst dosage (up to 1.0 g/L) can be described due to increased formation of free electrons and the decreased recombination rate of electron-hole pairs (e^-/h^+) in photocatalysis. Increasing CBZ efficiency under visible-light irradiation resulted from the increase in the total surface area available for the photocatalytic reaction [39]. However, the rate constant to the 0.5 g/L usages was similar to the 1.0 g/L usage, indicating the overdose photocatalysts might cause the aggregation of photocatalyst particles, consequently promoting the reduction effect of the surface-active site and shielding effect against light emission in the photocatalyst system [40,41]. Besides, given the overall treatment costs and process effectiveness, the photocatalyst loaded in the photoreactor system should be optimized. Thus, the 0.5 g/L photocatalysts dosage was used as an optimal dosage for CBZ degradation.

Based on the above discussions, we found AGO-1.0 could effectively remove CBZ, degrading CBZ completely in 30 min. Compared to other photocatalysts (Table 1), AGO-1.0 showed a better performance to degrade CBZ. The apparent rate constant was 0.12 min^{-1}, at the optimal condition: light intensity of 5.86 mW/cm^2, reaction temperature of 15–25 °C, pH of 5–7, and catalytic dosage of 0.5 g/L.

3.3. CBZ degradation mechanism and reaction paths

To estimate the photocatalytic degradation mechanism of CBZ over the Ag_3PO_4/GO photocatalyst under visible light irradiation, it is important to ascertain the dominant active species involved. To determine the effect of reactive oxygen species in the process, isopropanol (IPA, 10 mM), benzoquinone (BQ, 10 mM), and potassium iodide (KI, 10 mM) were added as scavengers to the CBZ solutions (5 mg/L) containing 0.2 g/L catalysts. IPA, BQ, and KI were used as scavengers of •OH, $•O_2^-$, and h^+, respectively [48–50]. As shown in Fig. 6a, the addition of KI or BQ in the system results in a fast deactivation in the CBZ degradation, while IPA added in the system shows a little inhibition. The effect of radical trapping agents on photocatalytic performances followed the order: KI > BQ > IPA. The effect of h^+ and $•O_2^-$ radical on the photocatalytic degradation of CBZ were the dominant mechanism, while •OH was also important to degrade CBZ. In addition, the ESR measurement was applied to identify the generation of •OH, $•O_2^-$, and h^+ during photocatalytic reaction caused by AGO-1.0 under 0 min dark condition and 5 min illumination. 5, 5-dimethyl-1-pyrroline-N-oxide (DMPO) could trap •OH and $•O_2^-$ as scavengers, while h^+ could react with 2, 2, 6, 6-Tetramethyl-1-piperidinyloxy (TEMPO) [51,52]. As displayed in Fig. 6b&c, strong characteristic peaks of DMPO-•OH and DMPO-$•O_2^-$ were observed, indicating that •OH and $•O_2^-$ were generated during the photocatalytic reaction [52]. And the weakening of TEMPO ESR signals under visible light irradiation indicated the existence of photogenerated h^+(Fig. 6d) [53]. Thus, h^+, $•O_2^-$, and •OH were the dominant radicals in the photocatalytic reaction.

To better identify the intermediates and illustrate the degradation pathway of CBZ, UPLC-MS was applied to determine the photodegradation process of CBZ by Ag_3PO_4/GO. Nine intermediates were detected, their m/z values and molecular structures were summarized in Table S2 and Fig. S6. The pathway of CBZ degradation by photocatalyst AGO-1.0 is shown in Fig. 7. CBZ (m/z = 237) was firstly transferred to TP252a due to the attack of $•O_2^-$ and h^+ [54,55]. There are two main pathways after forming TP252a. For pathway 1, TP252b was firstly formed from the epoxy bond cleavage of the TP252a [56]. TP252b was transformed to TP224 via cleavage reaction and ring contraction reaction [57]. Then TP224 was transferred into TP195 via decarboxylation processes [58]. For pathway 2, TP252a was further oxidized into TP259. Then TP259 was transferred into TP275 due to the attack on double bond in the central heterocyclic ring [59]. Finally, further degradation indicated ring-opening and produced TP151 and TP105.

The mechanism was proposed based on the above results and discussions, as shown in Fig. 8. Under the irradiation of visible light, photo-induced electron (e^-) transfer into the conduction band, and

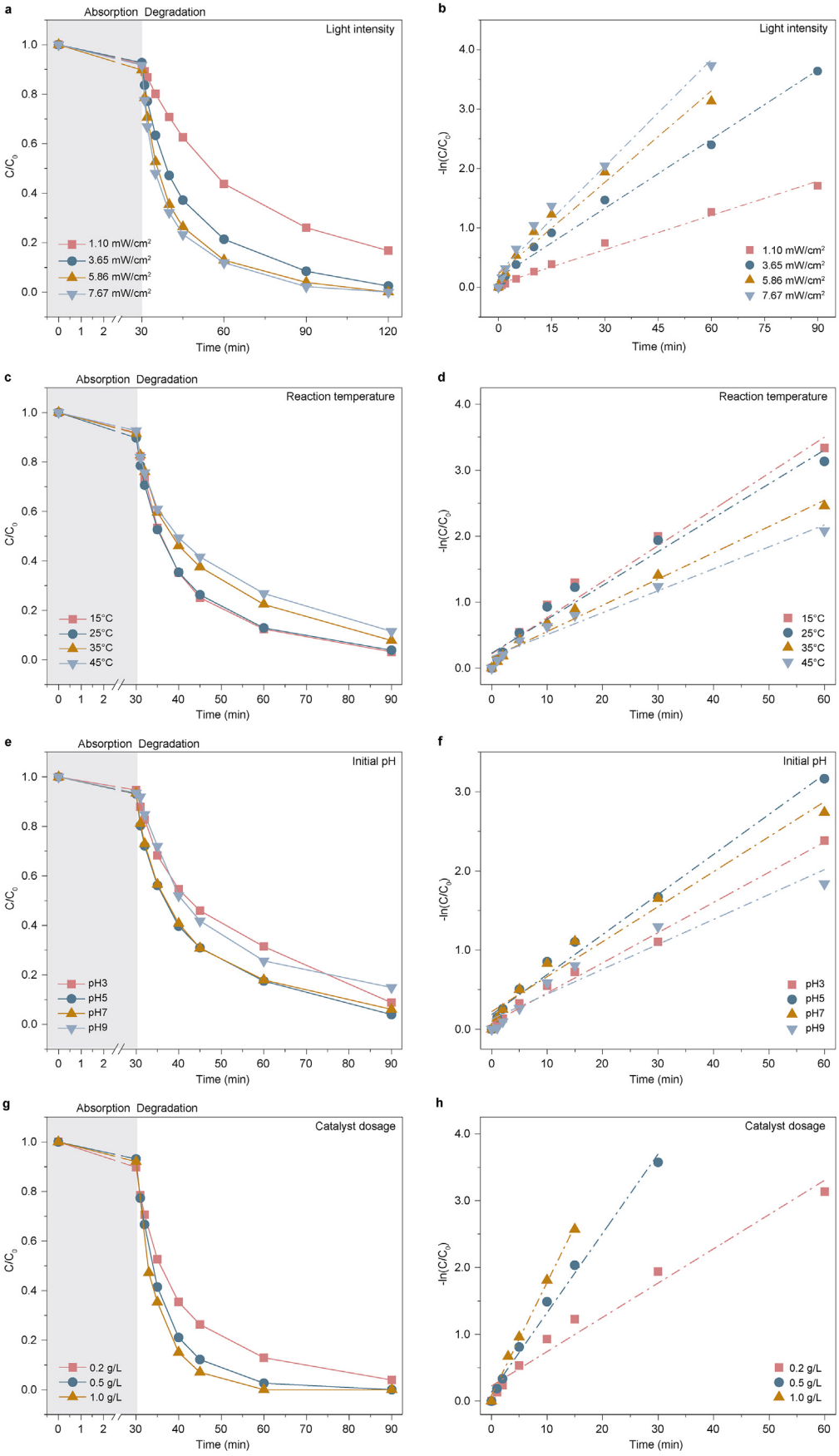
a
Absorption Degradation
Light intensity
C/C0
1.10 mW/cm²
3.65 mW/cm²
5.86 mW/cm²
7.67 mW/cm²
Time (min)
b
Light intensity
-ln(C/C0)
1.10 mW/cm²
3.65 mW/cm²
5.86 mW/cm²
7.67 mW/cm²
Time (min)
c
Absorption Degradation
Reaction temperature
C/C0
15°C
25°C
35°C
45°C
Time (min)
d
Reaction temperature
-ln(C/C0)
15°C
25°C
35°C
45°C
Time (min)
e
Absorption Degradation
Initial pH
C/C0
pH3
pH5
pH7
pH9
Time (min)
f
Initial pH
-ln(C/C0)
pH3
pH5
pH7
pH9
Time (min)
g
Absorption Degradation
Catalyst dosage
C/C0
0.2 g/L
0.5 g/L
1.0 g/L
Time (min)
h
Catalyst dosage
-ln(C/C0)
0.2 g/L
0.5 g/L
1.0 g/L
Time (min)

Fig. 5. (a–b) Effects of light intensity on CBZ degradation by AGO-1.0 (Experimental conditions: Catalytic dosage = 0.2 g/L, Reaction temperature = 25 °C, Initial pH = 6.8); (c–d) Effects of reaction temperature on CBZ degradation by AGO-1.0 (Experimental conditions: Light intensity = 5.86 mW/cm^2, Catalytic dosage = 0.2 g/L, Initial pH = 6.8); (e–f) Effects of initial pH on CBZ degradation by AGO-1.0 (Experimental conditions: Light intensity = 5.86 mW/cm^2, Catalytic dosage = 0.2 g/L, Reaction temperature = 25 °C); (g–h) Effects of catalyst dosage on CBZ degradation by AGO-1.0 (Experimental conditions: Light intensity = 5.86 mW/cm^2, Reaction temperature = 25 °C, Initial pH = 6.8).

Table 1
Photocatalytic decomposition of CBZ over various photocatalysts.

No.	Catalysts	Experimental conditions	k (min^{-1})	Ref.
1	$AgIO_3/BiVO_4$	CBZ = 5 mg/L; Catalyst dose = 1.0 g/L; Light intensity = 89 mW/cm^2	0.0896	[42]
2	PO_4/H-ZSM-5/BiOCl	CBZ = 2.5 mg/L; Catalyst dose = 0.8 g/L; Light = 350 W Xeon light	0.0634	[43]
3	BiOCl	CBZ = 2.5 mg/L; Catalyst dose = 0.5 g/L; Light = 350 W Xeon light	0.0237	[15]
4	TiO_2	CBZ = 2.5 mg/L; Catalyst dose = 0.5 g/L; Light = 350 W Xeon light	0.0025	[15]
5	Nd doped Sb_2O_3/TiO_2	CBZ = 5.0 mg/L; Catalyst dose = 0.5 g/L; Light = UVC	0.049	[16]
6	NCDs-BC-1[a]	CBZ = 5.0 mg/L; Catalyst dose = 0.8 g/L; Light = 500 W Xeon light	0.0281	[44]
7	MB20[b]	CBZ = 1.0 mg/L; Catalyst dose = 0.4 g/L; Light = 300 W Xeon light	0.0484	[45]
8	$M_3Cu_2^c$	CBZ = 20 mg/L; Catalyst dose = 0.3 g/L; Light = 300 W Xeon light	0.0563	[46]
9	FeBrCQDs-4[d]	CBZ = 10 mg/L; Catalyst dose = 0.6 g/L; Light = 50 W visible LED light	0.0381	[47]
10	**AGO-1.0**	**CBZ = 5 mg/L; Catalyst dose = 0.5 g/L; Light intensity = 5.86 mW/cm^2**	**0.12**	**This study**

Note: a. NCDs-BC-1, Nitrogen-doped carbon dots decorated on $BioBr/CeO_2$;
b. MB20, Ba embedded g-C_3N_4;
c. M_3Cu_2, $Mg_{0.3}Cu_{0.2}Zn_{0.5}Fe_2O_4$;
d. FeBrCQDs-4, $Fe_3O_4/_{BiOBr}$/CQDs.

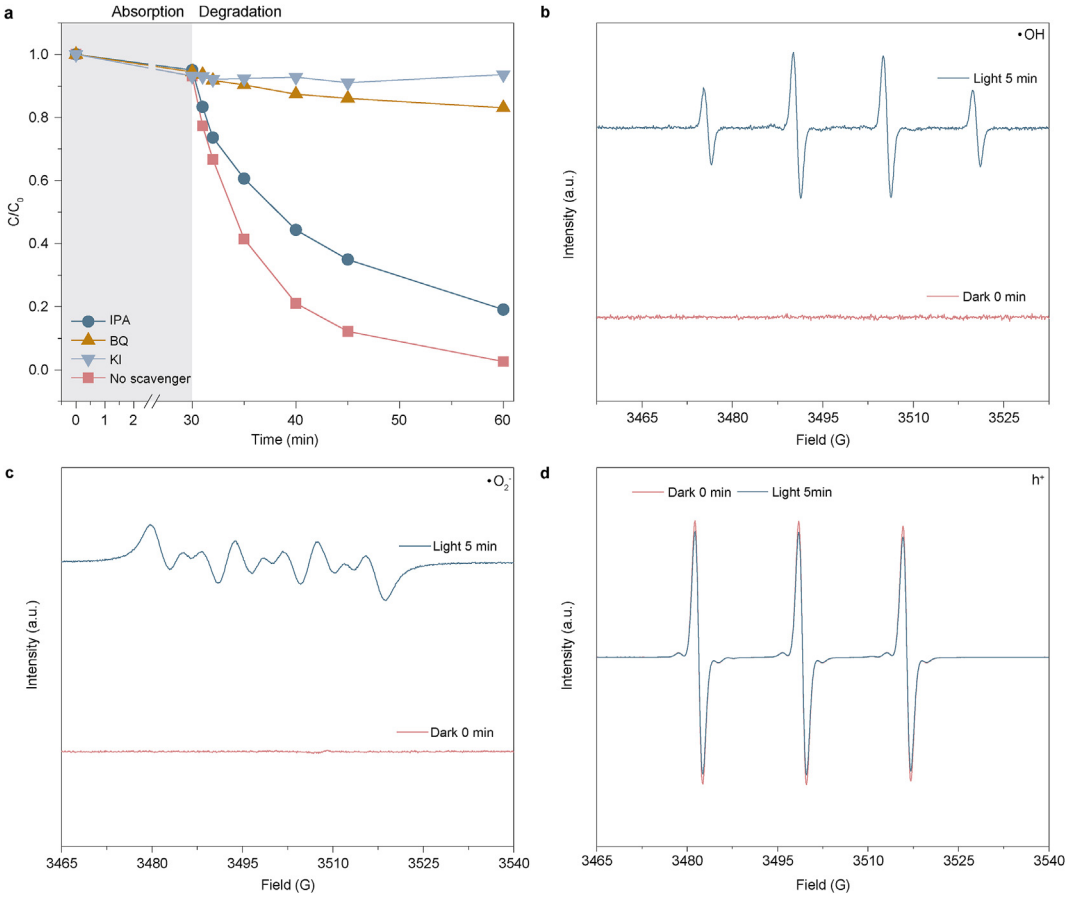

Fig. 6. (a) Radical trapping experiment of AGO-1.0 on CBZ degradation with different quenchers; The ESR spectra of radical adducts trapped by (b) DMPO- •OH, (c) DMPO- $\bullet O_2^-$, and (d) TEMPO-h^+.

hole (h^+) was formed in the valence band (Eq. (1)) [60]. Then the e^- in the conduction band transferred rapidly to the surface of GO sheets (Eq. (2)), and reacted with O_2 dissolved in water and formed the superoxide radicals ($O_2^-\bullet$) (Eq. (3)) [61]. Besides, hydroxyl radicals (•OH) would be formed when h^+ reacted with H_2O or OH^- (Eqs. (4) and (5)) [62]. Finally, CBZ would be removed and transferred to the ring-opening products by the oxidation of •OH and $O_2^-\bullet$ (Eq. (6)).

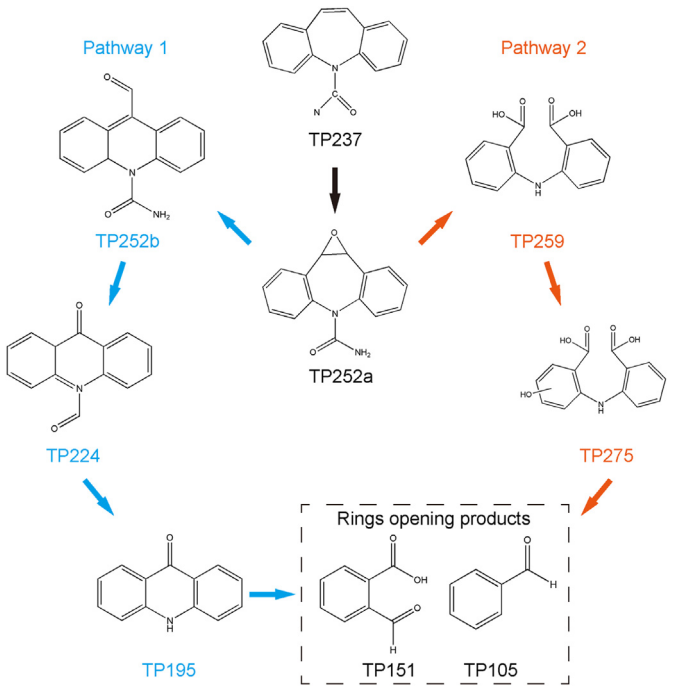

Fig. 7. The proposed pathway of CBZ degradation by AGO-1.0.

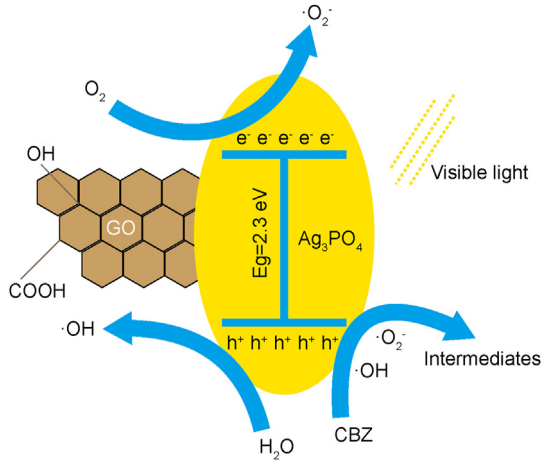

Fig. 8. The scheme of CBZ photodegradation by Ag_3PO_4/GO.

$$Ag_3PO_4 + h\nu \rightarrow h^+ + e^- \quad (1)$$

$$Ag_3PO_4(e^-_{CB}) \rightarrow GO(e^-_{CB}) \quad (2)$$

$$GO(e^-_{CB}) + O_2 \rightarrow \cdot O_2^- \quad (3)$$

$$h^+ + H_2O \rightarrow \cdot OH + H^+ \quad (4)$$

$$h^+ + OH^- \rightarrow \cdot OH \quad (5)$$

$$CBZ + h^+ + \cdot OH + \cdot O_2^- \rightarrow Intermediates \rightarrow H_2O + CO_2 \quad (6)$$

3.4. Stability of Ag_3PO_4/GO photocatalyst

In the practical application of photocatalyst in the degradation process, stability is a key criterion, so the stabilities of Ag_3PO_4, AGO-1.0 were investigated in this section. As shown in Fig. S7, the degradation percentage decreased significantly for 1 cycle and subsequently declined. And AGO-1.0 showed a small improvement than pure Ag_3PO_4, owing to the inhibition of photo-corrosion of Ag_3PO_4 by GO [63]. Besides, the XRD patterns of Ag_3PO_4 and AGO-1.0 after the photocatalytic tests could further confirm the inhibitory of GO on the photo-corrosion of Ag_3PO_4(Fig. S8). Combined with GO, the peaks of Ag were much smaller than neat Ag_3PO_4, suggesting GO could effectively prevent photo-corrosion of Ag_3PO_4.

4. Conclusions

Herein, an effective approach to remove CBZ was proposed by using photocatalyst AGO-1.0 under visible-light irradiation. GO would enhance the catalytic activity of Ag_3PO_4 over CBZ degradation through the visible-light utilization promotion and separation of electron-hole recombination of Ag_3PO_4. The effect of reaction parameters (light intensity, temperature, initial pH, and catalytic dosage) was comprehensively investigated, and the optimum conditions were as follows: the 5.86 mW/cm^2 light intensity, 15–25 °C temperature, 5–7 pH, and 0.5 mg/L catalytic dosage. At the optimum condition, CBZ could be removed effectively, and the pseudo-first-order rate constant reached 0.12 min^{-1}, which was 4 times higher than that of pristine Ag_3PO_4. The main reactive oxygen species were •OH and O_2•. Furthermore, the pathway of CBZ degradation by photocatalyst AGO-1.0 was also proposed to reveal the underlying mechanism, and the main products were the low-molecular products. This study provided a strategy to remove CBZ effectively and shed light on the remediation of refractory pollutants.

Declaration of competing interest

The authors declare that they have no known competing financial interests or personal relationships that could have appeared to influence the work reported in this paper.

Acknowledgment

This work was financially supported by Shenzhen Science and Technology Innovation Commission [No. KCXFZ202002011006362], National Natural Science Foundation of China [No. 52000051], and Initial Scientific Research Foundation of Overseas High-level Talents of Harbin Institute of Technology (Shenzhen) [No. FA11409005].

Appendix A. Supplementary data

Supplementary data to this article can be found online at https://doi.org/10.1016/j.ese.2021.100143.

References

[1] L.-J. Zhang, L. Qian, L.-Y. Ding, L. Wang, M.H. Wong, H.-C. Tao, Ecological and toxicological assessments of anthropogenic contaminants based on environmental metabolomics, Enivron. Sci. Ecotechnol. 5 (2021) 100081, https://doi.org/10.1016/j.ese.2021.100081.
[2] J. Cao, W. Nie, L. Huang, Y. Ding, K. Lv, H. Tang, Photocatalytic activation of sulfite by nitrogen vacancy modified graphitic carbon nitride for efficient degradation of carbamazepine, Appl. Catal. B Environ. 241 (2019) 18–27, https://doi.org/10.1016/j.apcatb.2018.09.007.
[3] C. Martínez, M. Canle L, M.I. Fernández, J.A. Santaballa, J. Faria, Kinetics and mechanism of aqueous degradation of carbamazepine by heterogeneous

photocatalysis using nanocrystalline TiO2, ZnO and multi-walled carbon nanotubes–anatase composites, Appl. Catal. B Environ. 102 (2011) 563–571, https://doi.org/10.1016/j.apcatb.2010.12.039.
[4] X. Yuan, S. Li, J. Hu, M. Yu, Y. Li, Z. Wang, Experiments and numerical simulation on the degradation processes of carbamazepine and triclosan in surface water: a case study for the Shahe Stream, South China, Sci. Total Environ. 655 (2019) 1125–1138, https://doi.org/10.1016/j.scitotenv.2018.11.290.
[5] M. Pierpaoli, A. Dettlaff, M. Szopińska, K. Karpienko, M. Wróbel, A. Łuczkiewicz, S. Fudala-Książek, R. Bogdanowicz, Simultaneous opto-electrochemical monitoring of carbamazepine and its electro-oxidation by-products in wastewater, J. Hazard Mater. 419 (2021) 126509, https://doi.org/10.1016/j.jhazmat.2021.126509.
[6] P. Somathilake, J.A. Dominic, G. Achari, C.H. Langford, J.-H. Tay, Use of low pressure mercury lamps with H2O2 and TiO2 for treating carbamazepine in drinking water: batch and continuous flow through experiments, J. Water Proc. Eng. 26 (2018) 230–236, https://doi.org/10.1016/j.jwpe.2018.10.015.
[7] Â. Almeida, A.M.V.M. Soares, V.I. Esteves, R. Freitas, Occurrence of the antiepileptic carbamazepine in water and bivalves from marine environments: a review, Environ. Toxicol. Pharmacol. 86 (2021) 103661, https://doi.org/10.1016/j.etap.2021.103661.
[8] X. Xin, G. Huang, X. Liu, C. An, Y. Yao, H. Weger, P. Zhang, X. Chen, Molecular toxicity of triclosan and carbamazepine to green algae Chlorococcum sp.: a single cell view using synchrotron-based Fourier transform infrared spectromicroscopy, Environ. Pollut. 226 (2017) 12–20, https://doi.org/10.1016/j.envpol.2017.04.007.
[9] M. Nkoom, G. Lu, J. Liu, H. Yang, H. Dong, Bioconcentration of the antiepileptic drug carbamazepine and its physiological and biochemical effects on Daphnia magna, Ecotoxicol. Environ. Saf. 172 (2019) 11–18, https://doi.org/10.1016/j.ecoenv.2019.01.061.
[10] E.-J. van den Brandhof, M. Montforts, Fish embryo toxicity of carbamazepine, diclofenac and metoprolol, Ecotoxicol. Environ. Saf. 73 (2010) 1862–1866, https://doi.org/10.1016/j.ecoenv.2010.08.031.
[11] A. Monteoliva-García, J. Martín-Pascual, M.M. Muñío, J.M. Poyatos, Effects of carrier addition on water quality and pharmaceutical removal capacity of a membrane bioreactor – Advanced oxidation process combined treatment, Sci. Total Environ. 708 (2020) 135104, https://doi.org/10.1016/j.scitotenv.2019.135104.
[12] S. Jemutai-Kimosop, F. Orata, V.O. Shikuku, V.A. Okello, Z.M. Getenga, Insights on adsorption of carbamazepine onto iron oxide modified diatomaceous earth: kinetics, isotherms, thermodynamics, and mechanisms, Environ. Res. 180 (2020) 108898, https://doi.org/10.1016/j.envres.2019.108898.
[13] J. Zhong, H. Jiang, Z. Wang, Z. Yu, L. Wang, J.F. Mueller, J. Guo, Efficient photocatalytic destruction of recalcitrant micropollutants using graphitic carbon nitride under simulated sunlight irradiation, Enivron. Sci. Ecotechnol. 5 (2021) 100079, https://doi.org/10.1016/j.ese.2021.100079.
[14] K.I. Ekpeghere, W.-J. Sim, H.-J. Lee, J.-E. Oh, Occurrence and distribution of carbamazepine, nicotine, estrogenic compounds, and their transformation products in wastewater from various treatment plants and the aquatic environment, Sci. Total Environ. (2018) 640–641, https://doi.org/10.1016/j.scitotenv.2018.05.218, 1015–1023.
[15] X. Gao, X. Zhang, Y. Wang, S. Peng, B. Yue, C. Fan, Rapid synthesis of hierarchical BiOCl microspheres for efficient photocatalytic degradation of carbamazepine under simulated solar irradiation, Chem. Eng. J. 263 (2015) 419–426, https://doi.org/10.1016/j.cej.2014.10.110.
[16] Z. Wang, V. Srivastava, S. Wang, H. Sun, S.K. Thangaraj, J. Jänis, M. Sillanpää, UVC-assisted photocatalytic degradation of carbamazepine by Nd-doped Sb2O3/TiO2 photocatalyst, J. Colloid Interface Sci. 562 (2020) 461–469, https://doi.org/10.1016/j.jcis.2019.11.094.
[17] D. Venieri, A. Fraggedaki, M. Kostadima, E. Chatzisymeon, V. Binas, A. Zachopoulos, G. Kiriakidis, D. Mantzavinos, Solar light and metal-doped TiO2 to eliminate water-transmitted bacterial pathogens: photocatalyst characterization and disinfection performance, Appl. Catal. B Environ. (2014) 154–155, https://doi.org/10.1016/j.apcatb.2014.02.007, 93–101.
[18] Y. Huang, X. Zhang, G. Zhu, Y. Gao, Q. Cheng, X. Cheng, Synthesis of silver phosphate/sillenite bismuth ferrite/graphene oxide nanocomposite and its enhanced visible light photocatalytic mechanism, Separ. Purif. Technol. 215 (2019) 490–499, https://doi.org/10.1016/j.seppur.2019.01.024.
[19] Z. Chen, W. Wang, Z. Zhang, X. Fang, High-efficiency visible-light-driven Ag $_3$ PO $_4$/AgI photocatalysts: Z-scheme photocatalytic mechanism for their enhanced photocatalytic activity, J. Phys. Chem. C 117 (2013) 19346–19352, https://doi.org/10.1021/jp406508y.
[20] L. Zhou, O.G. Alvarez, C.S. Mazon, L. Chen, H. Deng, M. Sui, The roles of conjugations of graphene and Ag in Ag3PO4-based photocatalysts for degradation of sulfamethoxazole, Catal. Sci. Technol. 6 (2016) 5972–5981, https://doi.org/10.1039/C6CY00192K.
[21] A.K. Geim, K.S. Novoselov, The rise of graphene, Nat. Mater. 6 (2007) 183–191, https://doi.org/10.1038/nmat1849.
[22] P.-Q. Wang, T. Chen, B. Yu, P. Tao, Y. Bai, Tollen's-assisted preparation of Ag3PO4/GO photocatalyst with enhanced photocatalytic activity and stability, J. Taiwan Inst. Chem. Eng. 62 (2016) 267–274, https://doi.org/10.1016/j.jtice.2016.02.016.
[23] V.-H. Nguyen, L.-A. Phan Thi, Q. Van Le, P. Singh, P. Raizada, P. Kajitvichyanukul, Tailored photocatalysts and revealed reaction pathways for photodegradation of polycyclic aromatic hydrocarbons (PAHs) in water, soil and other sources, Chemosphere 260 (2020) 127529, https://doi.org/10.1016/j.chemosphere.2020.127529.
[24] W. Chen, X. Niu, J. Wang, A photocatalyst of graphene oxide (GO)/Ag3PO4 with excellent photocatalytic activity over decabromodiphenyl ether (BDE-209) under visible light irradiation, J. Photochem. Photobiol. Chem. 356 (2018) 304–311, https://doi.org/10.1016/j.jphotochem.2017.12.038.
[25] S. Bai, X. Shen, H. Lv, G. Zhu, C. Bao, Y. Shan, Assembly of Ag3PO4 nanocrystals on graphene-based nanosheets with enhanced photocatalytic performance, J. Colloid Interface Sci. 405 (2013) 1–9, https://doi.org/10.1016/j.jcis.2013.05.023.
[26] P.-Q. Wang, T. Chen, B. Yu, P. Tao, Y. Bai, Tollen's-assisted preparation of Ag3PO4/GO photocatalyst with enhanced photocatalytic activity and stability, J. Taiwan Inst. Chem. Eng. 62 (2016) 267–274, https://doi.org/10.1016/j.jtice.2016.02.016.
[27] X. Guan, J. Shi, L. Guo, Ag3PO4 photocatalyst: hydrothermal preparation and enhanced O2 evolution under visible-light irradiation, Int. J. Hydrogen Energy 38 (2013) 11870–11877, https://doi.org/10.1016/j.ijhydene.2013.07.017.
[28] T.S. Anirudhan, V. Manjusha, F. Shainy, Magnetically retrievable cysteine modified graphene oxide@nickelferrite@titanium dioxide photocatalyst for the effective degradation of chlorpyrifos from aqueous solutions, Environ. Technol. Innovat. 23 (2021) 101633, https://doi.org/10.1016/j.eti.2021.101633.
[29] Y.A.J. Al-Hamadani, G. Lee, S. Kim, C.M. Park, M. Jang, N. Her, J. Han, D.-H. Kim, Y. Yoon, Sonocatalytic degradation of carbamazepine and diclofenac in the presence of graphene oxides in aqueous solution, Chemosphere 205 (2018) 719–727, https://doi.org/10.1016/j.chemosphere.2018.04.129.
[30] W. Chen, X. Niu, J. Wang, A photocatalyst of graphene oxide (GO)/Ag3PO4 with excellent photocatalytic activity over decabromodiphenyl ether (BDE-209) under visible light irradiation, J. Photochem. Photobiol. Chem. 356 (2018) 304–311, https://doi.org/10.1016/j.jphotochem.2017.12.038.
[31] S.-M. Huang, C.-H. Weng, J.-H. Tzeng, Y.-Z. Huang, J. Anotai, L.-T. Yen, C.-J. Chang, Y.-T. Lin, Kinetic study and performance comparison of TiO2-mediated visible-light-responsive photocatalysts for the inactivation of Aspergillus Niger, Sci. Total Environ. 692 (2019) 975–983, https://doi.org/10.1016/j.scitotenv.2019.07.329.
[32] M. Dilla, A. Mateblowski, S. Ristig, J. Strunk, Photocatalytic CO2 reduction under continuous flow high-purity conditions: influence of light intensity and H2O concentration, ChemCatChem 9 (2017) 4345–4352, https://doi.org/10.1002/cctc.201701189.
[33] B.O. Burek, D.W. Bahnemann, J.Z. Bloh, Modeling and optimization of the photocatalytic reduction of molecular oxygen to hydrogen peroxide over titanium dioxide, ACS Catal. 9 (2019) 25–37, https://doi.org/10.1021/acscatal.8b03638.
[34] Y. Liu, D. Yang, Y. Shi, L. Song, R. Yu, J. Qu, Z.-Z. Yu, Silver phosphate/graphene oxide aerogel microspheres with radially oriented microchannels for highly efficient and continuous removal of pollutants from wastewaters, ACS Sustain. Chem. Eng. 7 (2019) 11228–11240, https://doi.org/10.1021/acssuschemeng.9b00561.
[35] C. Xu, W. Yang, Q. Guo, D. Dai, M. Chen, X. Yang, Molecular hydrogen formation from photocatalysis of methanol on TiO2(110), J. Am. Chem. Soc. 135 (2013) 10206–10209, https://doi.org/10.1021/ja4030963.
[36] Z. Ghasemi, H. Younesi, A.A. Zinatizadeh, Kinetics and thermodynamics of photocatalytic degradation of organic pollutants in petroleum refinery wastewater over nano-TiO2 supported on Fe-ZSM-5, J. Taiwan Inst. Chem. Eng. 65 (2016) 357–366, https://doi.org/10.1016/j.jtice.2016.05.039.
[37] Y. Ma, J. Li, Y. Jin, K. Gao, H. Cai, G. Ou, The enhancement mechanism of ultra-active Ag3PO4 modified by tungsten and the effective degradation towards phenolic pollutants, Chemosphere 285 (2021) 131440, https://doi.org/10.1016/j.chemosphere.2021.131440.
[38] Y. Lin, S. Wu, X. Li, X. Wu, C. Yang, G. Zeng, Y. Peng, Q. Zhou, L. Lu, Microstructure and performance of Z-scheme photocatalyst of silver phosphate modified by MWCNTs and Cr-doped SrTiO3 for malachite green degradation, Appl. Catal. B Environ. 227 (2018) 557–570, https://doi.org/10.1016/j.apcatb.2018.01.054.
[39] S.-M. Huang, C.-H. Weng, J.-H. Tzeng, Y.-Z. Huang, J. Anotai, L.-T. Yen, C.-J. Chang, Y.-T. Lin, Kinetic study and performance comparison of TiO2-mediated visible-light-responsive photocatalysts for the inactivation of Aspergillus Niger, Sci. Total Environ. 692 (2019) 975–983, https://doi.org/10.1016/j.scitotenv.2019.07.329.
[40] K. Talukdar, B.-M. Jun, Y. Yoon, Y. Kim, A. Fayyaz, C.M. Park, Novel Z-scheme Ag3PO4/Fe3O4-activated biochar photocatalyst with enhanced visible-light catalytic performance toward degradation of bisphenol A, J. Hazard Mater. 398 (2020) 123025, https://doi.org/10.1016/j.jhazmat.2020.123025.
[41] L.K.B. Paragas, M.D.G. de Luna, R.-A. Doong, Rapid removal of sulfamethoxazole from simulated water matrix by visible-light responsive iodine and potassium co-doped graphitic carbon nitride photocatalysts, Chemosphere 210 (2018) 1099–1107, https://doi.org/10.1016/j.chemosphere.2018.07.109.
[42] Y. Zhang, J. Cui, H. Zhang, Y. Pei, Facile synthesis of a novel AgIO3/BiVO4 photocatalyst with two-step charge separation to enhance visible-light-driven photocatalytic performance for carbamazepine degradation, Separ. Purif. Technol. 276 (2021), 119273, https://doi.org/10.1016/j.seppur.2021.119273.
[43] X. Gao, X. Yang, Q. Guo, W. Peng, Y. Luo, Enhanced photocatalytic performance of BiOCl for carbamazepine degradation by coupling H-ZSM-5 and modifying phosphate groups: improved charge separation efficiency with high redox ability, J. Taiwan Inst. Chem. Eng. 104 (2019) 301–309, https://doi.org/

10.1016/j.jtice.2019.08.022.
[44] L. Liang, S. Gao, J. Zhu, L. Wang, Y. Xiong, X. Xia, L. Yang, The enhanced photocatalytic performance toward carbamazepine by nitrogen-doped carbon dots decorated on BiOBr/CeO2: mechanism insight and degradation pathways, Chem. Eng. J. 391 (2020) 123599, https://doi.org/10.1016/j.cej.2019.123599.
[45] J. Liang, W. Zhang, Z. Zhao, W. Liu, J. Ye, M. Tong, Y. Li, Different degradation mechanisms of carbamazepine and diclofenac by single-atom Barium embedded g-C3N4: the role of photosensitation-like mechanism, J. Hazard Mater. 416 (2021) 125936, https://doi.org/10.1016/j.jhazmat.2021.125936.
[46] P. Dhiman, M. Patial, A. Kumar, M. Alam, Mu Naushad, G. Sharma, D.-V.N. Vo, R. Kumar, Environmental friendly and robust Mg0.5-xCuxZn0.5Fe2O4 spinel nanoparticles for visible light driven degradation of Carbamazepine: band shift driven by dopants, Mater. Lett. 284 (2021), 129005, https://doi.org/10.1016/j.matlet.2020.129005.
[47] X. Xie, S. Li, K. Qi, Z. Wang, Photoinduced synthesis of green photocatalyst Fe3O4/BiOBr/CQDs derived from corncob biomass for carbamazepine degradation: the role of selectively more CQDs decoration and Z-scheme structure, Chem. Eng. J. 420 (2021) 129705, https://doi.org/10.1016/j.cej.2021.129705.
[48] Y. Zhang, A. Sun, M. Xiong, D.K. Macharia, J. Liu, Z. Chen, M. Li, L. Zhang, TiO2/BiOI p-n junction-decorated carbon fibers as weavable photocatalyst with UV−vis photoresponsive for efficiently degrading various pollutants, Chem. Eng. J. 415 (2021), 129019, https://doi.org/10.1016/j.cej.2021.129019.
[49] H. Zhu, Z. Chen, Y. Hu, L. Gong, D. Li, Z. Li, A novel immobilized Z-scheme P3HT/α-Fe2O3 photocatalyst array: study on the excellent photocatalytic performance and photocatalytic mechanism, J. Hazard Mater. 389 (2020) 122119, https://doi.org/10.1016/j.jhazmat.2020.122119.
[50] X. Jin, C. Wu, X. Tian, P. Wang, Y. Zhou, J. Zuo, A magnetic-void-porous MnFe2O4/carbon microspheres nano-catalyst for catalytic ozonation: preparation, performance and mechanism, Enivron. Sci. Ecotechnol. 7 (2021) 100110, https://doi.org/10.1016/j.ese.2021.100110.
[51] J. Gao, F. Zhang, H. Xue, L. Zhang, Y. Peng, X. Li, Y. Gao, N. Li, G. Lei, In-situ synthesis of novel ternary CdS/PdAg/g-C3N4 hybrid photocatalyst with significantly enhanced hydrogen production activity and catalytic mechanism exploration, Appl. Catal. B Environ. 281 (2021), 119509, https://doi.org/10.1016/j.apcatb.2020.119509.
[52] Z. Liu, L. Chen, C. Piao, J. Tang, Y. Liu, Y. Lin, D. Fang, J. Wang, Highly active Z-scheme WO3:Yb3+,Er3+/Ag/Ag3VO4/Ag photocatalyst with efficient charge transfer and light utilization for enhanced levofloxacin degradation with synchronous hydrogen evolution, Appl. Catal. Gen. 623 (2021) 118295, https://doi.org/10.1016/j.apcata.2021.118295.
[53] Y. Wu, X. Li, H. Zhao, F. Yao, J. Cao, Z. Chen, D. Wang, Q. Yang, Core-shell structured Cu2O@HKUST-1 heterojunction photocatalyst with robust stability for highly efficient tetracycline hydrochloride degradation under visible light, Chem. Eng. J. 426 (2021) 131255, https://doi.org/10.1016/j.cej.2021.131255.
[54] Y. Duan, L. Deng, Z. Shi, L. Zhu, G. Li, Assembly of graphene on Ag3PO4/AgI for effective degradation of carbamazepine under Visible-light irradiation: mechanism and degradation pathways, Chem. Eng. J. 359 (2019) 1379−1390, https://doi.org/10.1016/j.cej.2018.11.040.
[55] Q. Huo, X. Qi, J. Li, G. Liu, Y. Ning, X. Zhang, B. Zhang, Y. Fu, S. Liu, Preparation of a direct Z-scheme α-Fe2O3/MIL-101(Cr) hybrid for degradation of carbamazepine under visible light irradiation, Appl. Catal. B Environ. 255 (2019) 117751, https://doi.org/10.1016/j.apcatb.2019.117751.
[56] S. Begum, M. Ahmaruzzaman, CTAB and SDS assisted facile fabrication of SnO2 nanoparticles for effective degradation of carbamazepine from aqueous phase: a systematic and comparative study of their degradation performance, Water Res. 129 (2018) 470−485, https://doi.org/10.1016/j.watres.2017.11.031.
[57] G. Chen, H. Wang, W. Dong, Y. Huang, Z. Zhao, Y. Zeng, Graphene dispersed and surface plasmon resonance-enhanced Ag3PO4 (DSPR-Ag3PO4) for visible light driven high-rate photodegradation of carbamazepine, Chem. Eng. J. 405 (2021) 126850, https://doi.org/10.1016/j.cej.2020.126850.
[58] P.J. Mafa, M.E. Malefane, A.O. Idris, B.B. Mamba, D. Liu, J. Gui, A.T. Kuvarega, Cobalt oxide/copper bismuth oxide/samarium vanadate (Co3O4/CuBi2O4/SmVO4) dual Z-scheme heterostructured photocatalyst with high charge-transfer efficiency: enhanced carbamazepine degradation under visible light irradiation, J. Colloid Interface Sci. 603 (2021) 666−684, https://doi.org/10.1016/j.jcis.2021.06.146.
[59] J. Jiang, X. Wang, C. Zhang, T. Li, Y. Lin, T. Xie, S. Dong, Porous 0D/3D NiCo2O4/g-C3N4 accelerate emerging pollutant degradation in PMS/vis system: degradation mechanism, pathway and toxicity assessment, Chem. Eng. J. 397 (2020) 125356, https://doi.org/10.1016/j.cej.2020.125356.
[60] Y. Duan, L. Deng, Z. Shi, L. Zhu, G. Li, Assembly of graphene on Ag3PO4/AgI for effective degradation of carbamazepine under Visible-light irradiation: mechanism and degradation pathways, Chem. Eng. J. 359 (2019) 1379−1390, https://doi.org/10.1016/j.cej.2018.11.040.
[61] G. Chen, M. Sun, Q. Wei, Y. Zhang, B. Zhu, B. Du, Ag3PO4/graphene-oxide composite with remarkably enhanced visible-light-driven photocatalytic activity toward dyes in water, J. Hazard Mater. (2013) 244−245, https://doi.org/10.1016/j.jhazmat.2012.11.032, 86−93.
[62] P.-Q. Wang, T. Chen, B. Yu, P. Tao, Y. Bai, Tollen's-assisted preparation of Ag 3 PO 4/GO photocatalyst with enhanced photocatalytic activity and stability, J. Taiwan Inst. Chem. Eng. 62 (2016) 267−274, https://doi.org/10.1016/j.jtice.2016.02.016.
[63] Y. Liu, D. Yang, R. Yu, J. Qu, Y. Shi, H. Li, Z.-Z. Yu, Tetrahedral silver phosphate/graphene oxide hybrids as highly efficient visible light photocatalysts with excellent cyclic stability, J. Phys. Chem. C 121 (2017) 25172−25179, https://doi.org/10.1021/acs.jpcc.7b07848.